

I.V. STASYUK, I.R. DULEPA, O.V. VELYCHKO

Institute for Condensed Matter Physics, Nat. Acad. of Sci. of Ukraine  
(1, Svientsitskii Str., Lviv 79011, Ukraine)

## INVESTIGATION OF THE BOSONIC SPECTRUM OF TWO-DIMENSIONAL OPTICAL GRAPHENE-TYPE LATTICES. NORMAL PHASE

PACS 37.10.Jk, 67.85.-d

---

*The band spectrum of bosonic atoms in two-dimensional honeycomb optical lattices with the graphene-type structure has been studied. The dispersion laws in the bands and the one-particle spectral densities are calculated for the normal phase in the random phase approximation. The temperature-dependent gapless spectrum with Dirac points located at the Brillouin zone boundary is obtained for the lattice with energetically equivalent sites, with the corresponding chemical potential lying outside the allowed energy band. Different on-site energies in the sublattices are shown to induce the appearance of a gap in the spectrum, so that the chemical potential can be located between the subbands, which gives rise to a substantial reconstruction of the band spectrum. The frequency dependences of the one-particle spectral density for both sublattices are determined as functions of the chemical potential level, the spectral gap magnitude, and the temperature.*

*Keywords:* optical lattice, honeycomb lattice, phase transition, spectral density, hard-core bosons, Dirac points.

### 1. Introduction

Within the last decade, the considerable attention has been focused on the research and the description of the phenomena occurring at very low temperatures in subsystems of atoms that are located in the so-called optical lattices. Such lattices are created under laboratory conditions, using the interference of counter-propagating coherent laser beams [1, 2]. The electromagnetic field that arises in this case is periodic in space, with its period being determined by the length of light waves and the relative angle between the beams. As a result, the potential that acts on particles (atoms) in this field is also periodic. Atoms in the optical lattice compose a perfect quantum-mechanical system, almost all parameters of which can be controlled. This fact makes it possible to study phenomena which are hard to be observed in ordinary crystals. Depending on the number and the orientation of interfering beams, one-, two-, and three-dimensional lattices with various symmetries and structures can be created [3].

Two important directions of modern quantum physics were combined to research and to describe the behavior of ultracold Bose atoms in two-dimensional optical lattices with the honeycomb structure. On the

one hand, in optical lattices, phase transitions associated with the Bose condensation in the bosonic subsystem take place, and new phases of specific types can also emerge. An additional interest in such objects is related to the fact that a number of phenomena in the physics of condensed state and systems with strong particle correlations can be reproduced by analyzing the behavior of atoms arranged in optical lattices. On the other hand, a two-dimensional hexagonal carbon structure known as graphene became the object of a special attention recently. It has the unique physical properties resulting from the so-called Dirac energy spectrum of conduction electrons (a linear dispersion law in a vicinity of  $K$ -points in the Brillouin zone). Therefore, the study of the thermodynamics and the energy spectrum of Bose atoms, as well as Fermi ones, in optical lattices of the graphene type attracts a considerable attention. The corresponding important problems include, in particular, the research of how the mentioned feature in the energy spectrum affects the scenario of phase transitions in the system of ultra-cold atoms. The inverse problem concerning a modification of the spectrum structure at the transitions from one phase to the others is also of interest.

Quantum states in the system of bosonic atoms and a transition into the phase with the Bose con-

condensate (the so-called superfluid (SF) phase) in an optical lattice of the graphene type were observed in work [4]. The revealed regions of existence of various phases (in the case concerned, these were the Mott insulator and the SF phases) were in a qualitative agreement with the phase diagrams calculated in the mean-field approximation. The specification of phase region boundaries by making allowance for site-to-site correlations with the help of the cluster generalization of the Gutzwiller scheme was carried out later [5]. The attention was also paid to honeycomb lattices; here, in contrast to graphene, the states localized at the optical lattice sites are energetically nonequivalent if those sites belong to different sublattices,  $A$  and  $B$ . The cases of different on-site repulsion energies ( $U_A \neq U_B$ ) [6] and different potential well depths ( $\varepsilon_A \neq \varepsilon_B$ ) [7, 8] were examined. In the latter case, it was taken into consideration that, besides  $s$ -states of atoms, the excited  $p_{x,y}$ -states of atoms localized in deeper wells can also participate in the particle transfer and condensate formation processes. This circumstance made it possible to study mechanisms governing the formation of the so-called orbital (multiorbital) superfluid phase.

The features in the energy spectrum of bosons in optical lattices with the graphene-type structure were considered in a few works. In work [9], changes in the arrangement of Dirac points and the spectrum topology under the influence of the interaction between particles were considered, and the weak coupling approximation (in the framework of Bogolyubov's approach) was applied. In works [8, 10], the issues concerning the displacement and the possible disappearance of Dirac points as a result of the anisotropic ( $t_{ij} \neq t_{ij'}$ ) variations of parameters for the particle transfer between the neighbor lattice sites (such a variation can be stimulated by a mechanical shaking [10]) were analyzed; however, a more complete analysis of the spectrum and its reconstruction at transitions from one phases to the others was not carried out.

The theoretical description of the condensation of Bose particles in optical lattices in general and, in particular, in lattices with the graphene-type structure is mainly carried out on the basis of the Bose-Hubbard model [11, 12] and in its limiting ( $U \rightarrow \infty$ ) case, the hard-core boson model [13]. This model adequately describes the thermodynamics and the energy spectrum of a bosonic system at low population levels

( $0 \leq n \leq 1$ ). Being applied (in the simplest formulation) to honeycomb lattices, it enables one to find the boundaries of the regions, where the main phases exist: Mott insulator (MI), superfluid (SF) and modulated (CDW) phases; the latter exists if the sublattices are nonequivalent. The extension of the hard-core boson model by allowing the particle hopping  $t_{ij}$ , besides the nearest, to farther lattice sites, revealed the existence of new phases. As was shown in work [14], a large radius of the function  $t_{ij}$  gives rise to the appearance of a specific phase in the graphene-type lattice, the so-called Bose metal.

The hard-core boson model is known already since the 1950s. Its first application was associated with the liquid helium theory in the framework of the lattice model [15]. The model was also used in the theory of Josephson contact systems [16] and the theory of high-temperature superconductivity (in the local-pair approach) [17]. It was also made a basis for the calculations of ionic conductivity in crystals [18]. During last years, besides the description of the systems of ultracold Bose particles in optical lattices, the model was also applied to study the physical processes associated with ionic intercalation and adsorption of quantum particles on a metal surface [19, 20].

This work continues our theoretical researches [21–24] dealing with the energy spectrum and the spectral characteristics of a quantum lattice Bose gas, and, in particular, the hard-core boson model. In the framework of the pseudospin approach, by applying the fermionization procedure in the one-dimensional case [21] and the random phase approximation in the more general three-dimensional one [22], modifications in the one-particle spectral densities at the transition from the non-ordered (NO) state into the ordered one, in which  $\langle S^x \rangle = \langle b^+ \rangle = \langle b \rangle \neq 0$  and which is an analog of the phase with the lattice Bose condensate (the SF phase), were studied. The spectral densities and their frequency dependences obtained in work [22] qualitatively agree with the corresponding frequency dependences calculated on the basis of the fermionization model and using the method of exact diagonalization at one-dimensional clusters [23].

Our present research aimed at studying the spectral characteristics of a one-particle spectrum in the hard-core boson model in the case of a plane honeycomb (of the graphene type) lattice with energetically nonequivalent sites. A similar problem for a three-dimensional lattice with a model density of states

for the nonperturbed one-particle spectrum was considered in work [24], where some general regularities in the structure of the hard-core boson band spectrum were elucidated. The graphene-type lattice, however, introduces its specificity into the spectrum structure, and this issue had to be analyzed. We applied an approach expounded in works [22, 24]. It is based on the pseudo-spin formalism and the application of Green's function technique while calculating the spectral densities. At the first stage of calculations, the results of which are the topic of this paper, we found a band structure and one-particle spectral densities for the non-ordered (normal) phase and studied their dependences on the location level of the chemical potential of Bose particles with respect to the band spectrum, the difference between on-site energies,  $\delta = (\varepsilon_A - \varepsilon_B)/2$ , and the temperature.

## 2. Model

In the general case, the Hamiltonian of the quantum lattice gas is given by the expression

$$H = - \sum_{i,j} t_{ij} b_i^\dagger b_j + \sum_i (\varepsilon_\alpha - \mu) n_i, \quad (1)$$

where  $t_{ij}$  is the transfer integral,  $\varepsilon_\alpha$  are the on-site energies ( $\alpha = A$  or  $B$  is the sublattice index),  $\mu$  is the chemical potential,  $b_i^\dagger$  ( $b_i$ ) is the operator of particle creation (annihilation), and  $n_i$  is the number of particles at the  $i$ -th site. The site-to-site interaction energy is neglected.

In the case of optical lattices with deep potential wells, the energy of the on-site repulsion of Bose atoms is high, so that the hard-core boson model, in which the site population number is restricted ( $n_i = 0$  or  $1$ ), is a good approximation. Such bosons are described by the Pauli operators with the commutation relations

$$[b_i^+, b_j^+] = [b_i, b_j] = [b_i^+, b_j] = 0, \quad i \neq j; \quad \{b_i, b_i^+\} = 1. \quad (2)$$

The model becomes equivalent to the problem with the pseudospin  $S = \downarrow$  ( $S = \uparrow$ ) after the transformation

$$b_i^+ = S_i^-, \quad b_i = S_i^+, \quad b_i^+ b_i = n_i = \frac{1}{2} - S_i^z. \quad (3)$$

In the spin representation, the Hamiltonian looks like

$$H = - \sum_{i,j} t_{ij} S_i^- S_j^+ - \sum_i h_\alpha S_i^z + \text{const}, \quad (4)$$

where

$$h_\alpha = (\varepsilon_\alpha - \mu), \quad \text{const} = \sum_{\alpha=A,B} (\varepsilon_\alpha - \mu) \frac{N}{2}. \quad (5)$$

Below, the constant term in the Hamiltonian is omitted. The summation over  $i$  implies the summation over the cell index  $n$  and the sublattice index  $\alpha$ .

Taking the aforesaid into account, in the case of two sublattices ( $\alpha = A, B$ ), we obtain the following expression for the Hamiltonian:

$$\begin{aligned} H = & - \sum_{nn'} J_{nn'}^{AB} (S_{nA}^x S_{n'B}^x + S_{nA}^y S_{n'B}^y) - \\ & - \sum_{nn'} J_{nn'}^{BA} (S_{nB}^x S_{n'A}^x + S_{nB}^y S_{n'A}^y) - \\ & - h_A \sum_n S_{nA}^z - h_B \sum_{n'} S_{n'B}^z. \end{aligned} \quad (6)$$

Making a rotation by a certain angle  $\theta$  in the spin space,

$$\begin{aligned} S_{n\alpha}^z &= \sigma_{n\alpha}^z \cos \theta_\alpha + \sigma_{n\alpha}^x \sin \theta_\alpha \\ S_{n\alpha}^x &= \sigma_{n\alpha}^x \cos \theta_\alpha - \sigma_{n\alpha}^z \sin \theta_\alpha, \\ S_{n\alpha}^y &= \sigma_{n\alpha}^y, \end{aligned} \quad (7)$$

we obtain

$$\begin{aligned} H = & - \sum_{nn'} [L_1^{AB}(n, n') \sigma_{nA}^x \sigma_{n'B}^x + L_2^{AB}(n, n') \sigma_{nA}^z \sigma_{n'B}^z] + \\ & + \sum_{nn'} [L_3^{AB}(n, n') \sigma_{nA}^x \sigma_{n'B}^z + L_4^{AB}(n, n') \sigma_{nA}^z \sigma_{n'B}^x] - \\ & - \sum_{nn'} L_5^{AB}(n, n') \sigma_{nA}^y \sigma_{n'B}^y - \\ & - \sum_\alpha h_\alpha \sum_n (\sigma_{n\alpha}^z \cos \theta_\alpha + \sigma_{n\alpha}^x \sin \theta_\alpha), \end{aligned} \quad (8)$$

where the notations

$$\begin{aligned} L_1^{AB}(n, n') &= (J_{nn'}^{AB} + J_{n'n}^{BA}) \cos \theta_A \cos \theta_B, \\ L_2^{AB}(n, n') &= (J_{nn'}^{AB} + J_{n'n}^{BA}) \sin \theta_A \sin \theta_B, \\ L_3^{AB}(n, n') &= (J_{nn'}^{AB} + J_{n'n}^{BA}) \cos \theta_A \sin \theta_B, \\ L_4^{AB}(n, n') &= (J_{nn'}^{AB} + J_{n'n}^{BA}) \sin \theta_A \cos \theta_B, \\ L_5^{AB}(n, n') &= J_{nn'}^{AB} + J_{n'n}^{BA}. \end{aligned} \quad (9)$$

were introduced. Carrying out the Fourier transformation, we change to the wavevectors,

$$\begin{aligned} \sum_{n'} (J_{nn'}^{AB} + J_{n'n}^{BA}) e^{i\mathbf{q}(\mathbf{R}_{nA} - \mathbf{R}_{n'B})} &= \\ = J^{AB}(\mathbf{q}) \equiv J(\mathbf{q}), & \\ \sum_{n'} (J_{nn'}^{BA} + J_{n'n}^{AB}) e^{i\mathbf{q}(\mathbf{R}_{nB} - \mathbf{R}_{n'A})} &= \\ = J^{BA}(\mathbf{q}) \equiv J(-\mathbf{q}). & \end{aligned} \quad (10)$$

Then

$$\begin{aligned} L_1^{AB}(\mathbf{q}) &= J(\mathbf{q}) \cos \theta_A \cos \theta_B, \\ L_2^{AB}(\mathbf{q}) &= J(\mathbf{q}) \sin \theta_A \sin \theta_B, \\ L_3^{AB}(\mathbf{q}) &= J(\mathbf{q}) \cos \theta_A \sin \theta_B, \\ L_4^{AB}(\mathbf{q}) &= J(\mathbf{q}) \sin \theta_A \cos \theta_B, \\ L_5^{AB}(\mathbf{q}) &= J(\mathbf{q}). \end{aligned} \quad (11)$$

Taking into account that the environments of sites belonging to different sublattices are equivalent, we may write  $J^{AB}(0) = J^{BA}(0) \equiv J(0) = 3t$ , where  $t$  is the doubled transfer integral between neighbor lattice sites (see Appendix A). In the Hamiltonian, we single out a part that corresponds to the mean-field (MF) approximation,

$$\begin{aligned} \sigma_{nA}^\nu \sigma_{n'B}^{\nu'} &\rightarrow \langle \sigma_A^\nu \rangle \sigma_{n'B}^{\nu'} + \langle \sigma_B^{\nu'} \rangle \sigma_{nA}^\nu - \langle \sigma_A^\nu \rangle \langle \sigma_B^{\nu'} \rangle, \\ \nu, \nu' &= x, y, z, \langle \sigma_\alpha^x \rangle = \langle \sigma_\alpha^y \rangle = 0. \end{aligned} \quad (12)$$

As a result, the mean-field Hamiltonian reads

$$H_{\text{MF}} = - \sum_{n\alpha} E_\alpha \sigma_{n\alpha}^z. \quad (13)$$

The corresponding eigenvalues and the rotation angles  $\theta_\alpha$  are determined from the system of equations

$$\begin{aligned} E_\alpha &= (\varepsilon_\alpha - \mu) \cos \theta_\alpha - J(0) \langle S_\beta^x \rangle \sin \theta_\alpha, \\ (\varepsilon_\alpha - \mu) \sin \theta_\alpha + J(0) \langle S_\beta^x \rangle \cos \theta_\alpha &= 0, \end{aligned} \quad (14)$$

where

$$\begin{aligned} \langle S_\alpha^x \rangle &= - \langle \sigma_\alpha^z \rangle \sin \theta_\alpha, \quad \langle S_\alpha^z \rangle = \langle \sigma_\alpha^z \rangle \cos \theta_\alpha, \\ \langle \sigma_\alpha^z \rangle &= \frac{1}{2} \tanh \frac{\beta E_\alpha}{2}, \quad \alpha, \beta = A, B, \quad \alpha \neq \beta. \end{aligned} \quad (15)$$

In the non-ordered phase (for the system of bosons, this is the so-called normal phase),  $\theta_\alpha = 0$ ,  $\langle S_\alpha^x \rangle = 0$ ,  $\langle S_\alpha^z \rangle = \langle \sigma_\alpha^z \rangle$ , and  $E_\alpha = \varepsilon_\alpha$ . The solution  $\theta_\alpha \neq 0$  describes the ‘‘ordered’’ phase (the phase with the

condensate of hard-core bosons), for which  $\langle S_\alpha^x \rangle \equiv \langle b_\alpha \rangle \neq 0$  is the order parameter. The system of equations (14), together with formulas (15), determines the behavior of the order parameter and the average  $\langle S_\alpha^z \rangle$ , i.e.  $\langle n_\alpha \rangle$ , as the temperature in the ordered phase varies. The temperature-induced variation of the order parameter  $\langle S^x \rangle$  in the case where the crystal is not separated into sublattices [5], for the given on-site energy, and in the mean-field approximation is the same as in the Ising model with the transverse field acting on the spin (the role of the field in this work is played by the quantity  $h_\alpha = \varepsilon_\alpha - \mu$ ). In the further calculations, we will study the bosonic band spectrum in the non-ordered (NO) phase at a fixed temperature and its dependence on the fields  $h_\alpha$  at various distances from the curves on the phase diagrams (see work [24]) that correspond to the transitions into the phase with a Bose condensate (the SF phase).

### 3. Green's Functions and the Energy Spectrum of the Model

The one-particle energy spectrum can be calculated using the Green's function method and the random phase approximation. The one-particle Green's function on the operators  $\langle \langle b_{l\alpha} | b_{n\beta}^+ \rangle \rangle$  equals Green's function on the pseudospin operators  $\langle \langle S_{l\alpha}^+ | S_{n\beta}^- \rangle \rangle \equiv G_{l\alpha, n\beta}^{+-}$  [22, 24]:

$$\begin{aligned} \langle \langle S_{l\alpha}^+ | S_{n\beta}^- \rangle \rangle &= \langle \langle S_{l\alpha}^x | S_{n\beta}^x \rangle \rangle - i \langle \langle S_{l\alpha}^x | S_{n\beta}^y \rangle \rangle + \\ &+ i \langle \langle S_{l\alpha}^y | S_{n\beta}^x \rangle \rangle + \langle \langle S_{l\alpha}^y | S_{n\beta}^y \rangle \rangle. \end{aligned} \quad (16)$$

In the NO-phase ( $\cos \theta_\alpha = 1$ ,  $\sin \theta_\alpha = 0$ ),

$$\begin{aligned} G_{l\alpha, n\beta}^{+-} &= \langle \langle \sigma_{l\alpha}^x | \sigma_{n\beta}^x \rangle \rangle - i \langle \langle \sigma_{l\alpha}^x | \sigma_{n\beta}^y \rangle \rangle + \\ &+ i \langle \langle \sigma_{l\alpha}^y | \sigma_{n\beta}^x \rangle \rangle + \langle \langle \sigma_{l\alpha}^y | \sigma_{n\beta}^y \rangle \rangle. \end{aligned} \quad (17)$$

The equation of motion for Green's functions in the pseudospin component representation looks like

$$\hbar\omega \langle \langle \sigma_{l\alpha}^\nu | \sigma_{n\beta}^{\nu'} \rangle \rangle = \frac{\hbar}{2\pi} \langle [\sigma_{l\alpha}^\nu, \sigma_{n\beta}^{\nu'}] \rangle + \langle \langle [\sigma_{l\alpha}^\nu, H] | \sigma_{n\beta}^{\nu'} \rangle \rangle, \quad (18)$$

$\nu, \nu' = x, y$ .

Let us perform the decoupling of Green's function of the higher order, which corresponds to the random phase approximation. At this decoupling,  $[\sigma_{l\alpha}^z, H] \rightarrow$

$\rightarrow 0$  and, as a result,  $[\sigma_{l\alpha}^z, H] \rightarrow 0$ . For Green's functions with transverse pseudospin components, we obtain the system of equations

$$\begin{aligned} \hbar\omega \langle \langle \sigma_{l\alpha}^x | \sigma_{n\alpha}^x \rangle \rangle &= iE_\alpha \langle \langle \sigma_{l\alpha}^y | \sigma_{n\alpha}^x \rangle \rangle - \\ &- i \langle \sigma_\alpha^z \rangle \sum_n L_5^{\alpha\beta} \langle \langle \sigma_{n\beta}^y | \sigma_{n\alpha}^x \rangle \rangle, \\ \hbar\omega \langle \langle \sigma_{l\alpha}^y | \sigma_{n\alpha}^x \rangle \rangle &= -i \frac{\hbar}{2\pi} \langle \sigma_\alpha^z \rangle \delta_{ln} - iE_\alpha \langle \langle \sigma_{l\alpha}^x | \sigma_{n\alpha}^x \rangle \rangle + \\ &+ i \langle \sigma_\alpha^z \rangle \sum_n L_1^{\alpha\beta} \langle \langle \sigma_{n\beta}^x | \sigma_{n\alpha}^x \rangle \rangle, \\ \hbar\omega \langle \langle \sigma_{l\beta}^x | \sigma_{n\alpha}^x \rangle \rangle &= iE_\beta \langle \langle \sigma_{l\beta}^y | \sigma_{n\alpha}^x \rangle \rangle - \\ &- i \langle \sigma_\beta^z \rangle \sum_n L_5^{\beta\alpha} \langle \langle \sigma_{n\alpha}^y | \sigma_{n\alpha}^x \rangle \rangle, \\ \hbar\omega \langle \langle \sigma_{l\beta}^y | \sigma_{n\alpha}^x \rangle \rangle &= -iE_\beta \langle \langle \sigma_{l\beta}^x | \sigma_{n\alpha}^x \rangle \rangle + \\ &+ i \langle \sigma_\beta^z \rangle \sum_n L_1^{\beta\alpha} \langle \langle \sigma_{n\alpha}^x | \sigma_{n\alpha}^x \rangle \rangle, \end{aligned} \quad (19)$$

Hereafter,  $\alpha \neq \beta$ . The system of equations for the functions  $\langle \langle \sigma_{\dots}^x | \sigma_{n\alpha}^x \rangle \rangle$  has a similar form. After the Fourier transformation to the wave vectors,

$$G_{\alpha\beta}^{\nu\nu'}(\mathbf{q}) \equiv \sum_{l-n} \langle \langle \sigma_{l\alpha}^\nu | \sigma_{n\beta}^{\nu'} \rangle \rangle e^{i\mathbf{q}(\mathbf{R}_{l\alpha} - \mathbf{R}_{n\beta})}, \quad (20)$$

where  $L_1^{AB}(\mathbf{q}) = L_5^{AB}(\mathbf{q}) = J(\mathbf{q})$  and  $L_1^{BA}(\mathbf{q}) = L_5^{BA}(\mathbf{q}) = J(-\mathbf{q})$ , the system of equations (19) reads

$$\begin{aligned} \hbar\omega G_{\alpha\alpha}^{xx}(\mathbf{q}) &= iE_\alpha G_{\alpha\alpha}^{yx}(\mathbf{q}) - iJ(\mathbf{q}) \langle \sigma_\alpha^z \rangle G_{\beta\alpha}^{yx}(\mathbf{q}), \\ \hbar\omega G_{\alpha\alpha}^{yx}(\mathbf{q}) &= -i \frac{\hbar}{2\pi} \langle \sigma_\alpha^z \rangle - iE_\alpha G_{\alpha\alpha}^{xx}(\mathbf{q}) + \\ &+ iJ(\mathbf{q}) \langle \sigma_\alpha^z \rangle G_{\beta\alpha}^{xx}(\mathbf{q}), \\ \hbar\omega G_{\beta\alpha}^{xx}(\mathbf{q}) &= iE_\beta G_{\beta\alpha}^{yx}(\mathbf{q}) - iJ(-\mathbf{q}) \langle \sigma_\beta^z \rangle G_{\alpha\alpha}^{yx}(\mathbf{q}), \\ \hbar\omega G_{\beta\alpha}^{yx}(\mathbf{q}) &= -iE_\beta G_{\beta\alpha}^{xx}(\mathbf{q}) + iJ(-\mathbf{q}) \langle \sigma_\beta^z \rangle G_{\alpha\alpha}^{xx}(\mathbf{q}). \end{aligned} \quad (21)$$

The system of equations for Green's functions  $G_{\alpha\alpha}^{\nu y}(\mathbf{q})$  and  $G_{\beta\alpha}^{\nu y}(\mathbf{q})$  has a similar form (with the substitution  $J(\mathbf{q}) \rightarrow J(-\mathbf{q})$  at proper places). The sought Green's function is

$$G_{\alpha\alpha}^{+-}(\mathbf{q}) = \langle \langle b_\alpha | b_\alpha^+ \rangle \rangle_{\mathbf{q}} = G_{\alpha\alpha}^{+x}(\mathbf{q}) - iG_{\alpha\alpha}^{+y}(\mathbf{q}). \quad (22)$$

Here,

$$G_{\alpha\alpha}^{+x}(\mathbf{q}) = \langle \langle \sigma_\alpha^x | \sigma_\alpha^x \rangle \rangle_{\mathbf{q}} + i \langle \langle \sigma_\alpha^y | \sigma_\alpha^x \rangle \rangle_{\mathbf{q}}, \quad (23)$$

$$G_{\alpha\alpha}^{+y}(\mathbf{q}) = \langle \langle \sigma_\alpha^x | \sigma_\alpha^y \rangle \rangle_{\mathbf{q}} + i \langle \langle \sigma_\alpha^y | \sigma_\alpha^y \rangle \rangle_{\mathbf{q}}. \quad (24)$$

**892**

The equations given above have the following solutions:

$$G_{\alpha\alpha}^{\pm x}(\omega, \mathbf{q}) = \pm \frac{\hbar}{2\pi} \langle \sigma_\alpha^z \rangle \times \frac{\hbar\omega \mp E_\beta}{(\hbar\omega - E_\alpha)(\hbar\omega - E_\beta) - \langle \sigma_\alpha^z \rangle \langle \sigma_\beta^z \rangle |J(\mathbf{q})|^2}, \quad (25)$$

$$G_{\alpha\alpha}^{\pm y}(\omega, \mathbf{q}) = i \frac{\hbar}{2\pi} \langle \sigma_\alpha^z \rangle \times \frac{\hbar\omega \mp E_\beta}{(\hbar\omega - E_\alpha)(\hbar\omega - E_\beta) - \langle \sigma_\alpha^z \rangle \langle \sigma_\beta^z \rangle |J(\mathbf{q})|^2}. \quad (26)$$

The ultimate expressions for one-particle Green's functions are

$$G_{\beta\alpha}^{+-}(\omega, \mathbf{q}) = - \frac{\langle \sigma_\beta^z \rangle J(\mathbf{q})}{\hbar\omega - E_\beta} G_{\alpha\alpha}^{+-}(\omega, \mathbf{q}), \quad (27)$$

$$G_{\alpha\alpha}^{+-}(\omega, \mathbf{q}) = \frac{\hbar}{\pi} \langle \sigma_\alpha^z \rangle \times \frac{\hbar\omega - E_\beta}{(\hbar\omega - E_\alpha)(\hbar\omega - E_\beta) - \langle \sigma_\alpha^z \rangle \langle \sigma_\beta^z \rangle |J(\mathbf{q})|^2}. \quad (28)$$

In the normal phase, the spectrum of bosonic excitations determined from Eq. (28) looks like (see also work [24])

$$\begin{aligned} \varepsilon_{1,2}(\mathbf{q}) &= \frac{h_A + h_B}{2} \pm \\ &\pm \frac{1}{2} \sqrt{(h_A - h_B)^2 + 4 \langle \sigma_A^z \rangle \langle \sigma_B^z \rangle |J(\mathbf{q})|^2}, \end{aligned} \quad (29)$$

$$J(\mathbf{q}) = t \left( e^{iq_y a} + 2e^{-iq_y a} \cos\left(\frac{\sqrt{3}}{2} a q_x\right) \right)$$

(see Appendix A). Using the notations  $h = \frac{h_A + h_B}{2}$  and  $\delta = \frac{h_A - h_B}{2}$ , the expression for the spectrum can be written in the form

$$\varepsilon_{1,2}(\mathbf{q}) = h \pm \sqrt{\delta^2 + \frac{1}{9} \langle \sigma_A^z \rangle \langle \sigma_B^z \rangle J^2(0) |\gamma(\mathbf{q})|^2}. \quad (30)$$

The regions and the boundaries of existence for the normal (NO) phase, as well as for the phase with the Bose condensate (the SF phase), follow from the divergence condition for the function  $G_{\alpha\alpha}^{+-}$  at  $\omega \rightarrow 0$  and  $\mathbf{q} \rightarrow 0$ . The corresponding equation looks like

$$h^2 - \delta^2 = \langle \sigma_A^z \rangle \langle \sigma_B^z \rangle J^2(0) \equiv \langle \sigma_A^z \rangle \langle \sigma_B^z \rangle 9t^2. \quad (31)$$

The relevant  $(T, h)$  phase diagram in terms of  $J(0)$  units is plotted in Fig. 1.

#### 4. Spectrum of Bosonic Excitations. One-Particle Spectral Density of States

Let us determine the spectral density of bosonic excitations per one  $\alpha$ -sublattice site ( $\alpha = A, B$ ) for both sublattices as the imaginary part of Green's function  $\langle\langle b_{i\alpha}|b_{i\alpha}^+ \rangle\rangle_{\omega+i\varepsilon}$ :

$$\rho_\alpha(\omega) = -\frac{1}{N} \sum_{\mathbf{q}} \text{Im} \langle\langle b_\alpha|b_\alpha^+ \rangle\rangle_{\mathbf{q},\omega+i\varepsilon}. \quad (32)$$

On the basis of Eq. (28), we obtain

$$\rho_\alpha(\omega) = \frac{\langle\sigma_\alpha^z\rangle}{N} \sum_{\mathbf{q}} \left( C_1(\mathbf{q}) \delta\left(\omega - \frac{\varepsilon_1(\mathbf{q})}{\hbar}\right) + C_2(\mathbf{q}) \delta\left(\omega - \frac{\varepsilon_2(\mathbf{q})}{\hbar}\right) \right), \quad (33)$$

where the coefficients before  $\delta$ -functions equal

$$C_{1,2}(\mathbf{q}) = \frac{1}{2} \pm \frac{\delta_\alpha}{2\sqrt{\delta^2 + \frac{1}{9}\langle\sigma_\alpha^z\rangle\langle\sigma_\beta^z\rangle J^2(0)|\gamma(\mathbf{q})|^2}}. \quad (34)$$

Here,  $\alpha \neq \beta$ ,

$$\delta_\alpha = \begin{cases} \delta, & \alpha = A, \\ -\delta, & \alpha = B, \end{cases}$$

and  $\varepsilon_1(\mathbf{q})$  and  $\varepsilon_2(\mathbf{q})$  are the branches of spectrum (30). This expression for the spectral density in the NO phase formally coincides with that obtained in work [24] for the case of a cubic lattice.

The dependence of  $\rho_\alpha(\omega, \mathbf{q})$  on the wave vector is expressed through the dependence of  $J(\mathbf{q})$  on  $\mathbf{q}$ . The summation over  $\mathbf{q}$  is carried out within the limits of the first Brillouin zone  $\Omega$ . In order to calculate this sum, we change to the integral over the variable  $x \equiv |\gamma_{\mathbf{q}}|^2$  and introduce the function  $\rho_0(x)$ :

$$\begin{aligned} \frac{1}{N} \sum_{\mathbf{q} \in \Omega} \Phi(|J(\mathbf{q})|^2) &= \frac{1}{N} \sum_{\mathbf{q} \in \Omega} \Phi(t^2 |\gamma(\mathbf{q})|^2) = \\ &= \int dx \rho_0(x) \Phi(t^2 x), \\ \rho_0(x) &= \frac{1}{N} \sum_{\mathbf{q} \in \Omega} \delta(x - |\gamma(\mathbf{q})|^2). \end{aligned} \quad (35)$$

The transition from the summation over  $\mathbf{q}$  to the integration within the first Brillouin zone  $\Omega$  is done according to the formula

$$\frac{1}{N} \sum_{\mathbf{q} \in \Omega} (\dots) = \frac{S}{(2\pi)^2 N} \int dq_x dq_y (\dots), \quad (36)$$

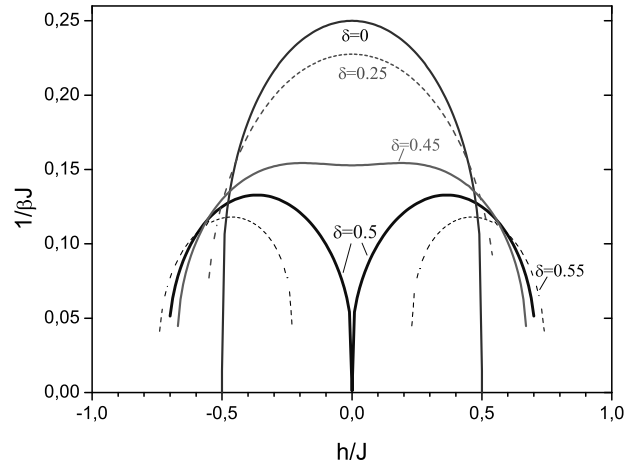


**Fig. 1.** Phase diagrams in the plane  $(T, h)$  for various values  $\delta = 0, 0.25, 0.45, 0.5$ , and  $0.55$  [24]. In this and other figures, all energy quantities are reckoned in  $J(0)$ -units

where  $S$  is the area of the so-called main crystal region, and  $N$  is the number of cells. The sense of the ratio  $S/N$  is the area of the elementary cell formed by the vectors  $\mathbf{a}_1$  and  $\mathbf{a}_2$  in the coordinate space:  $|\mathbf{a}_1| = |\mathbf{a}_2| = a\sqrt{3}$ ,  $\frac{S}{N} = \frac{3\sqrt{3}}{2}a^2$ .

Let us consider the integration limits over  $q_x$  and  $q_y$ . From Fig. 2, one can see that, instead of the integration over the region  $\Omega$ , it is possible to integrate within the limits of the marked rectangle. Since the integrand is an even function of the variables  $q_x$  and  $q_y$ , for the summation over  $\mathbf{q} \in \Omega$ , we have

$$\frac{1}{N} \sum_{\mathbf{q}} (\dots) = \frac{3\sqrt{3}a^2}{(2\pi)^2} \int_0^{\frac{2\pi}{\sqrt{3}a}} dq_x \int_0^{\frac{2\pi}{3a}} dq_y (\dots). \quad (37)$$

In terms of the variables  $2\vartheta = \frac{\sqrt{3}}{2}q_x a$  and  $\varphi = \frac{3}{2}q_y a$ , this formula looks like

$$\frac{1}{N} \sum_{\mathbf{q}} (\dots) = \frac{2}{\pi^2} \int_0^{\frac{\pi}{2}} d\vartheta \int_0^{\pi} d\varphi (\dots). \quad (38)$$

The final expression for  $\rho_0(x)$  in the case concerned has the form

$$\begin{aligned} \rho_0(x) &= \frac{1}{\pi^2} \int_0^{\pi} d\vartheta \int_0^{\pi} d\varphi \times \\ &\times \delta(x - 1 - 4 \cos 2\vartheta \cos \varphi - 4 \cos^2 2\vartheta). \end{aligned} \quad (39)$$

Formula (39) directly corresponds to the expression for the distribution function over the squared energy,  $g(\varepsilon^2)$ , for noninteracting particles in the lattice

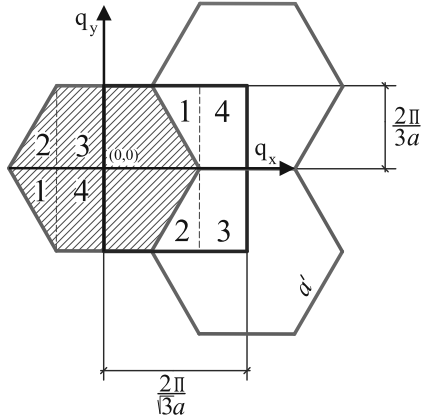


**Fig. 2.** First Brillouin zone  $\Omega$  in the reciprocal lattice (identical figures mark translationally equivalent regions)

with the graphene-type structure [25, 26], according to which  $\rho_0(x)$  can be expressed by means of the complete elliptic integral of the first kind,  $F(\frac{\pi}{2}, m)$ :

$$\rho_0(x) = \frac{1}{\pi^2} \frac{1}{\sqrt{Z_0}} F\left(\frac{\pi}{2}, \sqrt{\frac{Z_1}{Z_0}}\right), \quad (40)$$

where

$$Z_0 = \begin{cases} (1 + \sqrt{x})^2 - \frac{1}{4}(x - 1)^2, & x \leq 1, \\ 4\sqrt{x}, & 1 \leq x \leq 9; \end{cases}$$

$$Z_1 = \begin{cases} 4\sqrt{x}, & x \leq 1, \\ (1 + \sqrt{x})^2 - \frac{1}{4}(x - 1)^2, & 1 \leq x \leq 9. \end{cases}$$

The obtained function can be used to calculate the spectral density,

$$\rho_\alpha(\omega) = \langle \sigma_\alpha^z \rangle \int dx \rho_0(x) \left( C_1(x) \delta\left(\omega - \frac{\varepsilon_1(\mathbf{q})}{\hbar}\right) + C_2(x) \delta\left(\omega - \frac{\varepsilon_2(\mathbf{q})}{\hbar}\right) \right), \quad (41)$$

where

$$C_{1,2}(x) = \frac{1}{2} \left( 1 \pm \frac{\delta_\alpha}{\sqrt{\delta^2 + \langle \sigma_\alpha^z \rangle \langle \sigma_\beta^z \rangle t^2 x}} \right), \quad (42)$$

$$\langle \sigma_\alpha^z \rangle = \frac{1}{2} \tanh \frac{\beta h_\alpha}{2}. \quad (43)$$

For the  $\delta$ -functions in the expression for  $\rho_\alpha(\omega)$ , we use the formula  $\delta(f(x)) = \sum_i \frac{\delta(x-x_i)}{|f'(x_i)|}$ , where  $x_i$  are the roots of the equation  $f(x) = 0$ . In our case,

$$x_0 = \frac{(\hbar\omega - h)^2 - \delta^2}{\langle \sigma_\alpha^z \rangle \langle \sigma_\beta^z \rangle t^2}$$

is a root for both  $\delta$ -functions, with the first one giving a nonzero contribution at  $\hbar\omega > h$ , and the second one at  $\hbar\omega < h$ . The corresponding derivative

$$|f'(x_{1,2})| = \frac{t^2}{\hbar} \left| \frac{\langle \sigma_\alpha^z \rangle \langle \sigma_\beta^z \rangle}{2(\hbar\omega - h)} \right|.$$

After simplifications, we obtain

$$\rho_\alpha(\hbar\omega) = \frac{\rho_\alpha(\omega)}{\hbar} = \frac{\langle \sigma_\alpha^z \rangle}{t^2} \left( \rho_\alpha^{(1)}(\omega) + \rho_\alpha^{(2)}(\omega) \right). \quad (44)$$

Here, the spectral density per unit energy interval was introduced:

$$\rho_\alpha^{(1,2)}(\omega) = \rho_0(x_0) \left| \frac{\hbar\omega - h}{\langle \sigma_\alpha^z \rangle \langle \sigma_\beta^z \rangle} \right| \frac{\hbar\omega - h + \delta_\alpha}{\hbar\omega - h}, \quad (45)$$

$\alpha, \beta = A, B, \alpha \neq \beta$ .

The quantity  $\rho_\alpha^{(1)}(\omega)$  concerns the region  $\hbar\omega > h$ , and  $\rho_\alpha^{(2)}(\omega)$  the region  $\hbar\omega < h$ .

Let us consider the limits for the energies  $\varepsilon_1(x)$  and  $\varepsilon_2(x)$  of the band bosonic spectrum, if their argument changes in the interval  $0 \leq x \leq 9$ . For definiteness, let  $\delta$  be positive ( $\delta > 0$ ). The following cases are possible.

1)  $\langle \sigma_A^z \rangle \langle \sigma_B^z \rangle > 0$ .

This inequality is satisfied if  $h_A > 0$  and  $h_B > 0$  ( $h > 0$ ), or  $h_A < 0$  and  $h_B < 0$  ( $h < 0$ ) ( $h_A = h + \delta$ ,  $h_B = h - \delta$ ). The spectral density  $\rho_\alpha(\hbar\omega)$  differs from zero if

$$h - \sqrt{\delta^2 + 9\langle \sigma_A^z \rangle \langle \sigma_B^z \rangle t^2} \leq \hbar\omega \leq h - \delta \quad (46)$$

and

$$h + \delta \leq \hbar\omega \leq h + \sqrt{\delta^2 + 9\langle \sigma_A^z \rangle \langle \sigma_B^z \rangle t^2}. \quad (47)$$

The limits of the bands are given by the maximum and minimum values of the energies  $\varepsilon_2(x)$  and  $\varepsilon_1(x)$ , respectively. In the case concerned,

$$\begin{aligned} \min \varepsilon_1 &= \varepsilon_1(x=0) \equiv h + \delta, \\ \max \varepsilon_2 &= \varepsilon_2(x=0) \equiv h - \delta. \end{aligned} \quad (48)$$

Those energy values determine the spectral gap (the gap width  $\Delta\varepsilon = 2\delta$ ). The system is in the normal phase if the chemical potential  $\mu$  is located under the lower edge of the band  $\varepsilon_2(x)$ , provided that the energies  $h_A$  and  $h_B$  are positive or, if the energies  $h_A$  and  $h_B$  are negative, above the upper edge of the band  $\varepsilon_1(x)$ . The following conditions have to be satisfied:

$$\min \varepsilon_2 = \varepsilon_2(x=9) \equiv h - \sqrt{\delta^2 + 9\langle \sigma_A^z \rangle \langle \sigma_B^z \rangle t^2} > 0$$

in the former case, and

$$\max \varepsilon_1 = \varepsilon_1(x=9) \equiv h + \sqrt{\delta^2 + 9\langle\sigma_A^z\rangle\langle\sigma_B^z\rangle}t^2 < 0$$

in the latter one (in our model, the energy of bosons is always reckoned from the chemical potential level).

$$2) \langle\sigma_A^z\rangle\langle\sigma_B^z\rangle < 0.$$

At  $\delta > 0$ , this inequality takes place if  $h_A > 0$  and  $h_B < 0$  ( $h > 0$  or  $h < 0$ ). The band edges are determined now by the inequalities

$$h - \delta \leq \hbar\omega \leq h - \sqrt{\delta^2 - 9|\langle\sigma_A^z\rangle\langle\sigma_B^z\rangle|}t^2 \quad (49)$$

and

$$h + \sqrt{\delta^2 - 9|\langle\sigma_A^z\rangle\langle\sigma_B^z\rangle|}t^2 \leq \hbar\omega \leq h + \delta. \quad (50)$$

The spectral gap is confined by the values

$$\min \varepsilon_1 = \varepsilon_1(x=9) =$$

$$h + \sqrt{\delta^2 - 9|\langle\sigma_A^z\rangle\langle\sigma_B^z\rangle|}t^2 > 0,$$

$$\max \varepsilon_2 = \varepsilon_2(x=9) =$$

$$h - \sqrt{\delta^2 - 9|\langle\sigma_A^z\rangle\langle\sigma_B^z\rangle|}t^2 < 0 \quad (51)$$

and the gap width equals  $\Delta\varepsilon = 2(\delta^2 - 9|\langle\sigma_A^z\rangle\langle\sigma_B^z\rangle| \times t^2)^{1/2}$ . The chemical potential is located in the gap if the indicated inequalities are satisfied. The gap disappears at  $\delta = \pm 3t\sqrt{|\langle\sigma_A^z\rangle\langle\sigma_B^z\rangle|}$ .

The behavior of the functions  $\rho_\alpha(\hbar\omega)$  at the band edges is governed by both the distribution function  $\rho_0(x_0)$  with the frequency-dependent argument  $x_0$  and the multiplier to the right from  $\rho_0(x_0)$  on the right-hand side of formula (45). When approaching the band edges (including the case  $x_0 \rightarrow 0$ , which corresponds to the limiting transition  $\hbar\omega \rightarrow h \pm \delta$ ), the function  $\rho_0(x_0)$  tends to a finite value of  $\frac{1}{\pi\sqrt{3}}$ . This fact follows from formula (14), because, in this limit,  $Z_1(x_0)/Z_0(x_0) \rightarrow 0$ ,  $\sqrt{Z_0(x_0)} \rightarrow \frac{\sqrt{3}}{2}$ , and  $F(\pi/2, 0) = \frac{\pi}{2}$ .

On the other hand,

$$\hbar\omega - h + \delta_\alpha \rightarrow \begin{cases} 1, & \hbar\omega \rightarrow h + \delta_\alpha, \\ 0, & \hbar\omega \rightarrow h - \delta_\alpha. \end{cases}$$

Therefore,

$$\rho_A(\hbar\omega) \rightarrow \begin{cases} \frac{2}{t^2} \frac{\delta}{|\langle\sigma_A^z\rangle\langle\sigma_B^z\rangle|} \langle\sigma_A^z\rangle \frac{1}{\pi\sqrt{3}}, & \hbar\omega \rightarrow h + \delta, \\ 0, & \hbar\omega \rightarrow h - \delta; \end{cases} \quad (52)$$

$$\rho_B(\hbar\omega) \rightarrow \begin{cases} 0, & \hbar\omega \rightarrow h + \delta, \\ \frac{2}{t^2} \frac{\delta}{|\langle\sigma_A^z\rangle\langle\sigma_B^z\rangle|} \langle\sigma_B^z\rangle \frac{1}{\pi\sqrt{3}}, & \hbar\omega \rightarrow h - \delta. \end{cases}$$

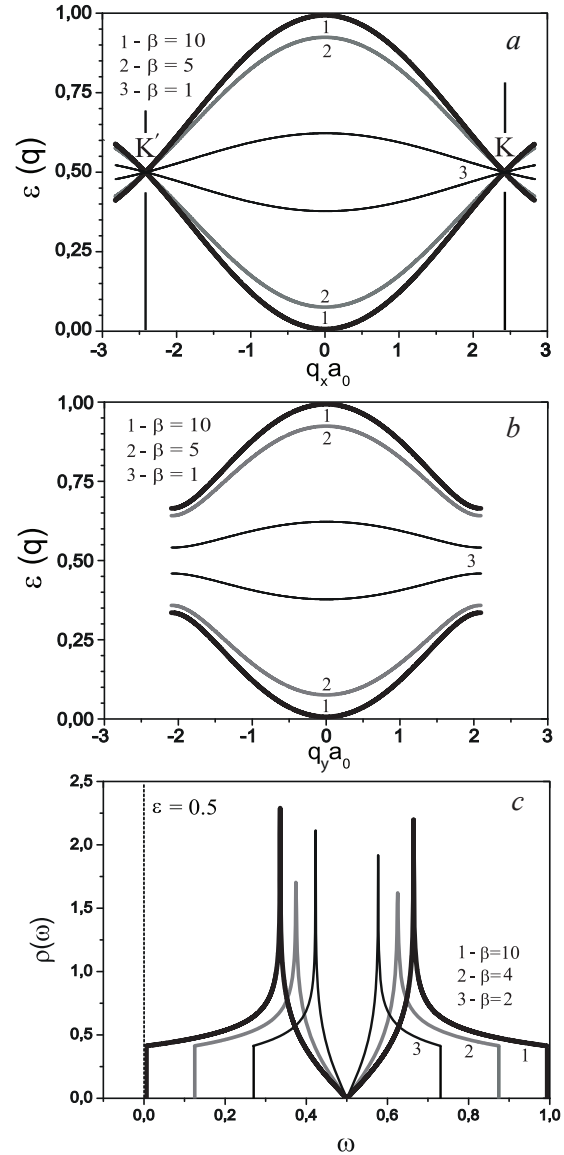


**Fig. 3.** Dispersion laws of bosonic excitations in the honeycomb lattice (a and b) and the frequency dependence of the one-particle spectral density of states  $\rho(\omega)$  (c) in the case  $\delta = 0$  and for the one-particle energy  $\varepsilon = 0.5$ . One partial spectral density of states was obtained for the temperatures  $\beta = 10, 4$ , and 2 ( $\langle n_\alpha \rangle = \frac{1}{2} - \langle \sigma_\alpha^z \rangle$ ,  $\langle n_\alpha \rangle_{\beta=10} = 0.0066$ ,  $\langle n_\alpha \rangle_{\beta=4} = 0.1192$ ,  $\langle n_\alpha \rangle_{\beta=2} = 0.2689$ )

Expanding each of the functions  $Z_0(x)$ ,  $Z_1(x)$ , and  $F(\pi/2, m)$  in a series in its argument, when the latter is small, it can be convinced that, if the deviations from the points where  $\rho_{A,B} = 0$  are small, those functions linearly increase with the frequency. In all

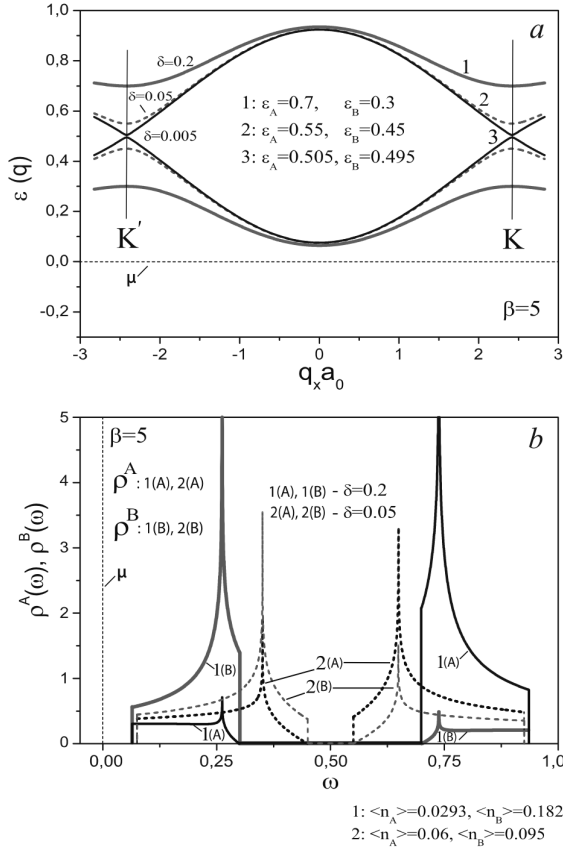


**Fig. 4.** (a) Dispersion laws  $\varepsilon(\mathbf{q})$  in the NO phase calculated for  $\beta = 5$  and  $\delta = 0.005, 0.05$ , and  $0.2$ . The chemical potential level ( $\mu = 0$ ) is located below the band spectrum (dashed curve). (b) Frequency dependences of the one-particle spectral density for sublattices  $A$  and  $B$  calculated for  $\beta = 5$  and  $\delta = 0.2$  and  $0.05$

other cases, the function  $\rho_A(\hbar\omega)$  and  $\rho_B(\hbar\omega)$  become equal to zero at the band edges in a jump-like manner.

Numerical calculations according to formula (45) and making allowance for expressions (15) for the average  $\langle \sigma_A^z \rangle$  and  $\langle \sigma_B^z \rangle$  confirm the described topology of spectral densities. In particular, in case (1) where the chemical potential is located under or above both bands, the spectral density has a jump on one side of the gap and grows smoothly on the other side. If the chemical potential is located in the gap, the spectral density has jumps on both gap sides. The general and well-known property of the Bose–Hubbard model is that the spectral densities  $\rho_A$  and  $\rho_B$  are negative in the region with  $\hbar\omega < 0$  (i.e. below the chemical

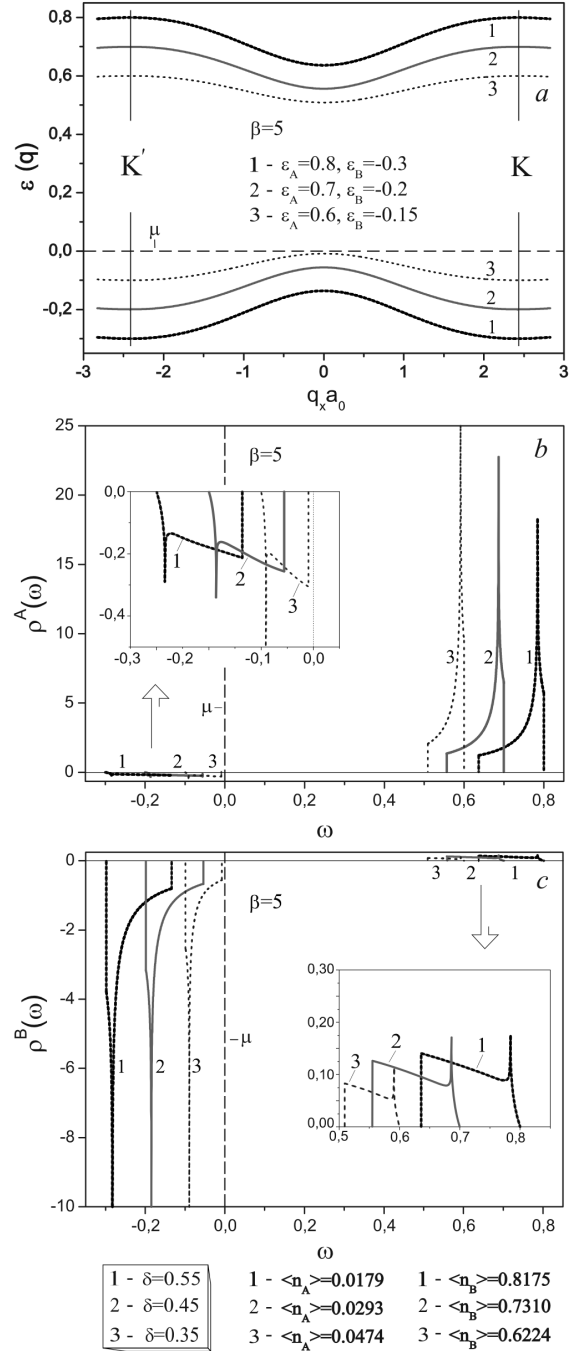


**Fig. 5.** Dispersion laws for the NO phase at various values of half-difference between one-particle energies  $d = 0.35, 0.45$ , and  $0.55$  (a), and one-particle spectral density of states for sublattices  $A$  (b) and  $B$  (c) for the indicated  $\varepsilon_A$ - and  $\varepsilon_B$ -values. The average population numbers of sites in the elementary cell,  $\langle n_\alpha \rangle$  ( $\alpha = A, B$ ), are given. The dashed curve marks the chemical potential level ( $\mu = 0$ )

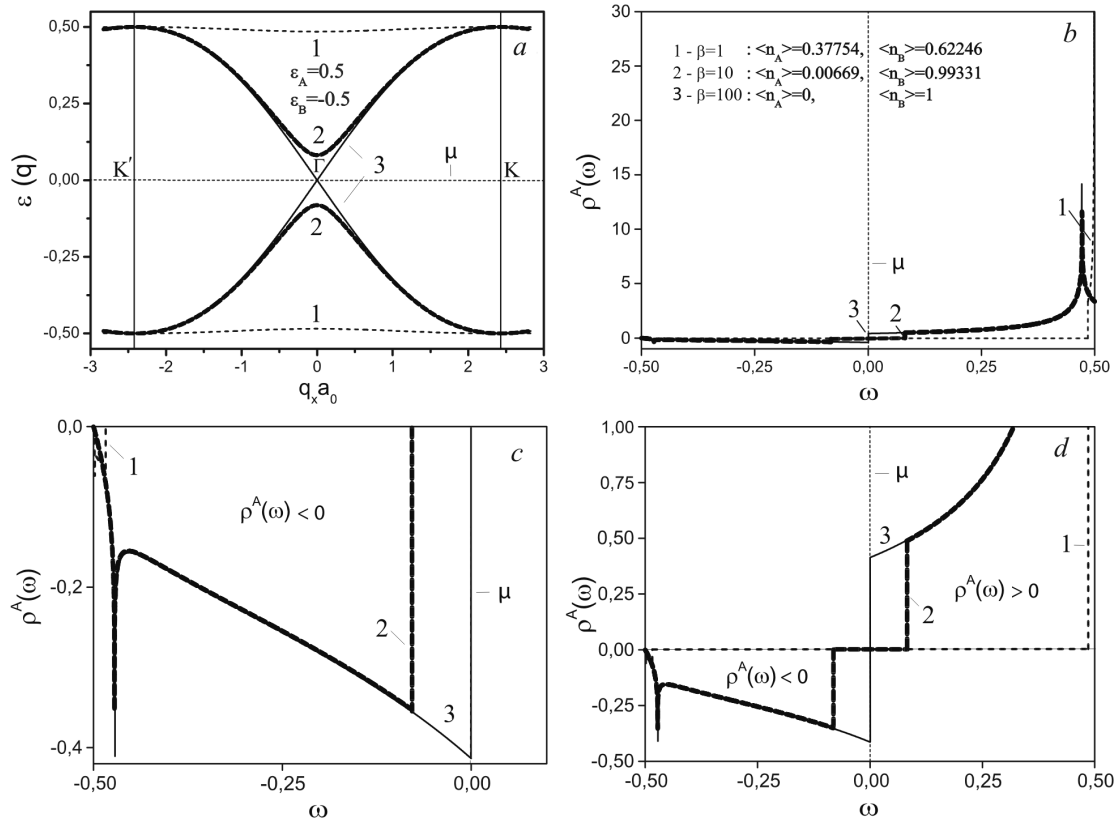


**Fig. 6.** (a) Dispersion laws  $\varepsilon(\mathbf{q})$  ( $\delta = 0.5$ ) for the temperatures  $\beta = 1, 10$ , and  $100$  (the critical temperature  $kT_c = 0$ ) in the NO phase. (b) One-particle spectral density of states for sublattice A,  $\rho^A(\omega)$ . The chemical potential level is located at the gap middle-point. (c and d) Scaled-up regions of panel b

potential level) and positive in the region with  $\hbar\omega > 0$  (above  $\mu$ ).

For a honeycomb lattice of the graphene type, the spectrum of bosonic excitations is gapless ( $\Delta\varepsilon = 0$ ) if the depths of potential wells are identical ( $\varepsilon_A = \varepsilon_B$ ). Figures 3, a and b illustrate the temperature-induced variation of the spectral gap width: as the temperature decreases, the band width increases and reaches a maximum at the temperature of the phase transition into the state with a Bose condensate. Two spectral branches touch each other at Dirac points  $K$  and  $K'$  in the Brillouin zone corners.

The dispersion law of bosonic excitations for another cross-section of the energy surface for the spectrum along the axis  $q_y$  within the limits of the first Brillouin zones (the component  $q_x = 0$ ) is shown in Fig. 3, b. Here, two spectral branches do not coincide at the Brillouin zone boundary. In the case concerned ( $\delta = 0, \varepsilon_A = \varepsilon_B = 0.5$ ), the one-particle spec-

tral density for various temperatures was obtained (Fig. 3, c). In vicinities of the Dirac points, the energy spectrum changes linearly (Fig. 3, a).

In the case of different potential well depths ( $\varepsilon_A \neq \varepsilon_B$ ), the gap mentioned above emerges at the Brillouin zone boundary. The gap width is determined by the difference between the on-site energies. Figure 4, a illustrates the energy spectrum of bosonic excitations at the inverse temperature  $\beta = 5$ . Small differences between the on-site energies  $\delta = 0.005, 0.05$ , and  $0.2$  ( $\varepsilon_A \neq \varepsilon_B > 0$ ) were considered. The spectral gap magnitude  $\Delta\varepsilon = 2\delta$ , and the gap limits are  $\hbar\omega_{1,2} = h \pm \delta$ . For the spectrum of bosonic excitations located above the chemical potential level  $\mu$ , the calculated spectral densities are positive (Figs. 3, b and 4, b), and, in the case where the bands are located under the  $\mu$ -level, they are negative. The limiting frequency values that confine the interval, where  $\rho_\alpha(\hbar\omega) \neq 0$ , equal  $\hbar\omega_{3,4} = h \pm \sqrt{\delta^2 + \langle\sigma_A^z\rangle\langle\sigma_B^z\rangle J^2(0)}$ .

In the case where the chemical potential level lies between the bands (see Fig. 5, *a* corresponding to the same inverse temperature  $\beta = 5$ ), the behavior of the energy spectrum of bosonic excitations is essentially different. The extrema of spectral branches at  $\mathbf{q} = 0$  are oriented toward the chemical potential level  $\mu$ . The negative values of one-particle spectral density ( $\rho(\hbar\omega) < 0$ ) correspond to the lower band located under the chemical potential level  $\mu$ , and the positive ones to the upper band (Figs. 5, *b* and *c*).

From the  $(T, h)$  phase diagram (Fig. 1), one can see that the point of the phase transition between the NO and SF phases, where the SF phase becomes separated into two regions, corresponds to the critical gap value in the spectrum of bosonic excitations,  $\Delta(kT_c) = 2\delta_c = 1$  (in  $J(0)$ -units). Figure 6, *a* (the corresponding  $\delta = 0.5$ ) illustrates the behavior of the energy spectrum of bosonic excitations at various temperatures in the case where the chemical potential level is located at the band midpoint. At the inverse temperature  $\beta = 100$  (practically, this is the absolute zero temperature), two spectral branches practically touch each other at the zone center (at  $\mathbf{q} = 0$ ); this situation corresponds to the point of the phase transition NO  $\rightarrow$  SF for  $d = 0.5$  and  $\beta_c \rightarrow \infty$ . The average population number for Bose particles at a site in the sublattice *A*,  $\langle n_A \rangle = 0$ , whereas in the sublattice *B*,  $\langle n_B \rangle = 1$ . The figure also demonstrates the forms of the one-particle spectral density of states at the *A*-site for the values  $\beta = 1$  and 10, and near the critical point at  $\beta = 100$  ( $kT_c \simeq 0$ ) (panels *b* to *d*).

The character of changes in the frequency dependence of the one-particle spectral density of states, which depends on the location of the chemical potential level, qualitatively agrees with the results of calculations obtained in the framework of the exact diagonalization technique for the one-dimensional chain model [23]. In the cited work, the hoppings of hard-core bosons onto neighbor sites were considered, and negative values were obtained for the one-particle spectral densities at energies located below the chemical potential level.

## 5. Conclusions

On the basis of the hard-core boson model, the energy spectrum of bosonic excitations and the one-particle spectral densities were calculated for a plane honeycomb lattice of the graphene type. The features in the

band spectrum structure and the spectral density in the normal (NO) phase, as well as their dependences on the location of the chemical potential level, the difference between the local energies of particles in the sublattices, and the temperature, are considered.

Conditions for the appearance of a gap in the band spectrum are analyzed. It is found that, in the case of hard-core bosons when particles are described by the Pauli statistics, there emerges a temperature-dependent gap (in contrast to electrons in graphene-type lattices). The spectral gap  $\Delta\varepsilon$  exists:

- at the edge of the Brillouin zone, if the chemical potential level is located below (above) the energy bands; in this case,  $\Delta\varepsilon = 2\delta$ ;

- at  $\mathbf{q} = 0$ , if the chemical potential level lies between the energy bands; in this case,  $\Delta\varepsilon = 2\sqrt{\delta^2 - |\langle \sigma_A^z \rangle \langle \sigma_B^z \rangle| J^2(0)}$ .

In the former case, the gap disappears at  $\delta = 0$ . As a result, there appear the Dirac points with a linear dispersion law at points *K* and *K'* of the Brillouin zone. In the latter case, the gap becomes zero at  $kT = 0$ ,  $h = 0$ , and  $\delta = \frac{1}{2}J(0)$  ( $\delta = \frac{1}{2}$  in  $J(0)$ -units). A linear spectrum of the Dirac type,  $\varepsilon_{\mathbf{q}} \sim \frac{J(0)}{2\sqrt{2}}aq$ , also emerges in this case

The profiles of the calculated spectral densities correspond to general criteria: the densities are negative in the interval  $\omega < 0$  and positive at  $\omega > 0$ . The specificity of the honeycomb lattice structure manifests itself in the available logarithmic singularities in the curves  $\rho_{\alpha}(\hbar\omega)$  for each band and in a jump-like zeroing at the spectrum edges (except for the points  $\hbar\omega = h - \delta_{\alpha}$ , where the density tends to zero linearly).

The results of our research can serve as a basis for the description of the thermodynamics of Bose atoms in hexagonal optical lattices and the further study of their dynamics (experimental means that allow the features in the energy spectrum and the spectral densities of ultracold atoms in the systems of this type to be revealed directly include the interband and momentum-resolved Bragg spectroscopies [27, 28]). For the ultimate solution of the problem to be obtained, it is necessary to consider the case of the SF phase (with a Bose condensate). Unlike the normal phase, the chemical potential in the SF phase is located in either of the energy bands. As a result, a considerable reconstruction of the bosonic spectrum associated with the appearance of additional subbands occurs [24, 29, 30]. The corresponding cal-

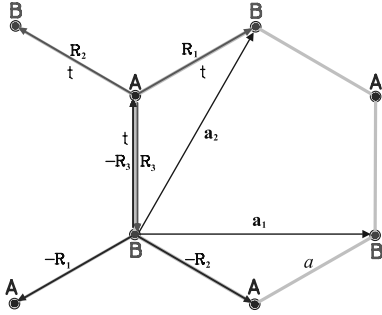


**Fig. 7.** Nearest neighbours for sites in sublattices  $A$  and  $B$

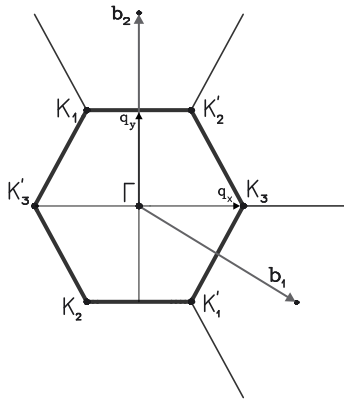


**Fig. 8.** First Brillouin zone.  $\mathbf{b}_1$  and  $\mathbf{b}_2$  are the translation vectors

calculations of the dispersion laws in the bands and the spectral densities for a lattice of the graphene type will be the subject of our separate consideration.

## APPENDIX A Graphene-Type Honeycomb Lattice

The two-dimensional graphene-type honeycomb optical lattice is obtained as a result of the interference of three coherent laser beams [8] oriented at an angle of  $2\pi/3$  with respect to each other and with the sum of their wave vectors being equal to zero,  $\mathbf{k}_1 + \mathbf{k}_2 + \mathbf{k}_3 = 0$ . This lattice include two triangular sublattices  $A$  and  $B$  shifted with respect to each other by the vector  $\frac{(\mathbf{a}_1 + \mathbf{a}_2)}{3}$ . The elementary cell of the lattice contains two sites, one per each sublattice. For this lattice (Fig. 7), the translation vectors are

$$\mathbf{a}_1 = (a\sqrt{3}, 0), \quad \mathbf{a}_2 = \left(a\frac{\sqrt{3}}{2}, \frac{3}{2}a\right). \quad (\text{A1})$$

A honeycomb lattice has a hexagonal Brillouin zone in the inverse space of wave vectors. This is a regular hexagon with two nonequivalent points  $K$  and  $K'$  at the zone corners

(Fig. 8). The corresponding translation vectors are

$$\mathbf{b}_1 = \left(\frac{1}{\sqrt{3}a}, \frac{1}{3a}\right), \quad \mathbf{b}_2 = \left(0, \frac{2}{3a}\right), \quad (\text{A2})$$

where  $|\mathbf{b}_1| = |\mathbf{b}_2| = \frac{2}{3a}$ , and  $a$  is the distance between the neighbor sites in the direct lattice. The distance from the Brillouin zone center to points  $K$  and  $K'$  equals  $\frac{4\pi}{3\sqrt{3}a}$ .

While considering the energy spectrum of quantum particles (bosons) arranged in the optical lattice, the strong coupling approach can be used. It is based on the consideration of particle hoppings between the neighbor sites describing by the parameter  $t$ , which is connected with the overlapping of the wave functions of Bose particles that are localized at those sites. The coordination number of every atom  $z = 3$ :

$$\mathbf{R}_1 = \left(\frac{a\sqrt{3}}{2}, \frac{a}{2}\right), \quad \mathbf{R}_2 = \left(-\frac{a\sqrt{3}}{2}, \frac{a}{2}\right), \quad \mathbf{R}_3 = (0, -a). \quad (\text{A3})$$

The Fourier transforms of the nearest-neighbor hopping energy calculated in two cases –  $A \Rightarrow B$  ( $J^{AB}(\mathbf{q})$ ) and  $B \Rightarrow A$  ( $J^{BA}(\mathbf{q})$ ) – differ by the sign before the vectors  $\mathbf{R}_c$  (Fig. 7):

$$J^{AB}(\mathbf{q}) = t \sum_{c=1}^3 e^{i\mathbf{q}\mathbf{R}_c}, \quad J^{BA}(\mathbf{q}) = t \sum_{c=1}^3 e^{-i\mathbf{q}\mathbf{R}_c}. \quad (\text{A4})$$

Hence, we obtain

$$J^{AB}(\mathbf{q}) = t \left( e^{-iq_y a} + 2 \cos\left(\frac{\sqrt{3}}{2}q_x a\right) e^{i\frac{q_y a}{2}} \right) \equiv J(\mathbf{q}),$$

$$J^{BA}(\mathbf{q}) \equiv J(-\mathbf{q}) \quad (\text{A5})$$

and, in the general case, the dimensionless parameter associated with the transfer  $A \Rightarrow B$  between the nearest sites looks like

$$\begin{aligned} \gamma(\mathbf{q}) &= \frac{\sqrt{|J^{AB}(\mathbf{q})J^{BA}(\mathbf{q})|}}{t} = \\ &= \sqrt{1 + 4 \cos\left(\frac{\sqrt{3}}{2}q_x a\right) \cos\left(\frac{3}{2}q_y a\right) + 4 \cos^2\left(\frac{\sqrt{3}}{2}q_x a\right)}. \end{aligned} \quad (\text{A6})$$

Note that  $\gamma(\mathbf{q}) = 0$  at points  $K$  and  $K'$  of the Brillouin zone.

1. M. Greiner, O. Mandel, T. Esslinger, T.W. Hänsch, and I. Bloch, *Nature* **415**, 39 (2002).
2. M. Greiner, O. Mandel, T.W. Hänsch, and I. Bloch, *Nature* **419**, 51 (2002).
3. I. Bloch, *Nature Phys.* **1**, 23 (2005).
4. P. Soltau-Panahi, J. Struck, A. Bick, W. Plenkers, G. Meineke, C. Becker, P. Windpassinger, K. Sengstock, P. Hauke, and M. Lewenstein, *Nature Phys.* **7**, 434 (2011).
5. D.-S. Lühmann, *Phys. Rev. A* **87**, 043619 (2013).
6. Q.-Q. Lu and J.-M. Hou, *Commun. Theor. Phys.* **53**, 861 (2010).
7. P. Soltau-Panahi, D.-S. Lühmann, J. Struck, P. Windpassinger, and K. Sengstock, *Nature Phys.* **8**, 71 (2012).
8. E. Albus, X. Fernandez-Gonzalvo, J. Mur-Petit, J.J. Garcia-Ripoli, and J.K. Pachos, *Ann. Phys.* **328**, 64 (2013).
9. Z. Chen and B. Wu, *Phys. Rev. Lett.* **107**, 065301 (2011).
10. S. Koghee, L.-K. Lim, M.O. Goerbig, and C. Morais-Smith, *Phys. Rev. A* **85**, 023637 (2012).

11. M.P.A. Fisher, P.B. Weichman, G. Grinstein, and D.S. Fisher, *Phys. Rev. B* **40**, 546 (1989).
12. D. Jaksch, C. Bruder, J.I. Cirac, C.W. Gardiner, and P. Zoller, *Phys. Rev. Lett.* **81**, 3108 (1998).
13. R.T. Whitlock and P.R. Zilsel, *Phys. Rev.* **131**, 2409 (1963).
14. C.N. Varney, K. Sun, V. Galitski, and M. Rigol, *New J. Phys.* **14**, 115028 (2012).
15. T. Matsubara and H. Matsuda, *Progr. Theor. Phys.* **16**, 569 (1956); **17**, 19 (1957).
16. G.A. Czathy, J.D. Reppy, and M.H.W. Chan, *Phys. Rev. Lett.* **91**, 235301 (2003).
17. S. Robashkiewicz, R. Micnas, and K.A. Chao, *Phys. Rev. B* **23**, 1447 (1981); **24**, 1579 (1981).
18. G.D. Mahan, *Phys. Rev. B* **14**, 780 (1976).
19. M.J. Puska and R.M. Nieminen, *Surf. Sci.* **157**, 413 (1985).
20. W. Brenig, *Surf. Sci.* **291**, 207 (1993).
21. I.V. Stasyuk and I.R. Dulepa, *Condens. Matter Phys.* **10**, 259 (2007).
22. I.V. Stasyuk and I.R. Dulepa, *J. Phys. Studies* **13**, 2701 (2009).
23. I.V. Stasyuk, O. Vorobyov, and R.Ya. Stetsiv, *Ferroelectrics* **426**, 6 (2012).
24. I.V. Stasyuk and O. Vorobyov, *Condens. Matter Phys.* **16**, 23005 (2013).
25. H.B. Rosestock, *J. Chem. Phys.* **16**, 2064 (1953).
26. J.P. Hobson and W.A. Nierenberg, *Phys. Rev.* **89**, 662 (1953).
27. P.T. Ernst, S. Götze, J.S. Krauser, K. Pyka, D.-S. Lühmann, D. Pfannkuche, and K. Sengstock, *Nature Phys.* **6**, 56 (2010).
28. N. Fabbri, S.D. Huber, D. Clément, L. Fallani, C. Fort, M. Inguscio, and E. Altman, *Phys. Rev. Lett.* **109**, 055301 (2012).
29. Y. Ohashi, M. Kitaura, and H. Matsumoto, *Phys. Rev. A* **73**, 033617 (2006).
30. C. Menotti and N. Trivedi, *Phys. Rev. B* **77**, 235120 (2008).

Received 24.02.14.

Translated from Ukrainian by O.I. Voitenko

*I.V. Стасюк, І.Р. Дулепа, О.В. Величко*

ДОСЛІДЖЕННЯ БОЗОННОГО  
СПЕКТРА ДВОВИМІРНИХ ОПТИЧНИХ  
ҐРАТОК ЗІ СТРУКТУРОЮ ТИПУ  
ГРАФЕНУ. НОРМАЛЬНА ФАЗА

Резюме

Досліджено зонний спектр бозе-атомів у двовимірних гексагональних оптичних ґратках із структурою типу графену. У наближенні хаотичних фаз розраховано для нормальної фази закони дисперсії в зонах та одночастинкові спектральні густини. Для ґратки з енергетично еквівалентними вузлами отримано температурно залежний безщільний спектр з точками Дірака на краю зони Бріллюена. Хімічний потенціал розташований у цьому випадку поза дозволеною енергетичною зоною. При відмінності між енергіями частинок на вузлах різних підґраток, коли виникає щільна у спектрі, хімічний потенціал може перебувати між підзонами. У такому разі має місце значна перебудова зонного спектра. Визначено частотні залежності одночастинкових спектральних густин для обидвох підґраток залежно від розміщення рівня хімічного потенціалу, величини щільності у зонному спектрі та температури.